Two-Photon Phosphorescence Lifetime Microscopy

4

Nastaran Abbasizadeh and Joel A. Spencer

4.1 Background

Due to the central role of oxygen in several physiological and pathological conditions, different strategies have been developed over the years to enable the quantitative or semi-quantitative measurement of oxygen in the blood and tissues. These strategies include approaches such as electron paramagnetic resonance (EPR), nitroimidazole (e.g., pimonidazole) adduct staining, microelectrodes, and optical sensors [5–7]. Although EPR has provided some signs of progress towards measuring free radicals and oxygen in biological systems, its usage in human subjects is challenging due to complex instrumentation (e.g., the need for magnets with a large air gap and adequate homogeneity in the magnetic-field), probe administration (placing an exogenous probe in the desired location), and regulatory issues for human applications (e.g., obtaining approval for indefinite embedding of the probes in the tissue) [8–11]. Nitroimidazoles can be used to determine whether cells have been in hypoxia (below ~10 mmHg), but they provide an indirect measurement of hypoxia and can only be used for a single timepoint measurement due to the destructive biopsy required for tissue preparation and measurement [12–14]. Alternatively, Clark-type electrodes, devised by Leland Clark in 1953, can provide robust and quantitative oxygen tension measurements in the whole blood and tissue [15]. As an electrochemical sensor, Clark-type electrodes have shown several advantages over other sensors such as good stability and high reproducibility, but they can also suffer from limitations like oxygen consumption and needle

N. Abbasizadeh · J. A. Spencer (✉)
Department of Bioengineering, University of California Merced, Merced, CA, USA

NSF-CREST Center for Cellular and Biomolecular Machines and the Health Science Research Institute, University of California Merced, Merced, CA, USA
e-mail: joel.spencer@ucmerced.edu

X. Wei, B. Gu (eds.), *Optical Imaging in Human Disease and Biological Research*, Advances in Experimental Medicine and Biology 1355,
https://doi.org/10.1007/978-981-15-7627-0_4

sensor-induced damage to the tissue [16–18]. Optical techniques, such as phosphorescence lifetime quenching microscopy, can provide fast, quantitative oxygen sensing non-invasively in living biological samples without oxygen consumption, making it an optimal alternative to the methods described above [18]. Furthermore, phosphorescence lifetime quenching measurements do not show the luminophore concentration-dependency associated with intensity measurements. This is especially important in the context of measuring oxygen tension inside tissues and cells with heterogeneous distributions of probes and depth-dependent signal loss that can invalidate intensity-based measurements. 2PLM is a relatively new version of phosphorescence lifetime quenching microscopy for non-invasive sensing of the partial pressure of oxygen (pO_2) with high spatial and temporal resolution.

Historically, "optical sensing" of oxygen was initiated with the Kautsky and Hirsch work in the 1930s in which they reported the quenching of phosphorescence in traces of oxygen. In this experiment, they monitored room temperature phosphorescence of dyes immobilized on silica gel and observed light emission only when there was no oxygen present [19]. This method was later used by Pringsheim et al. [20] to measure oxygen production as low as 5×10^{-8} cm^3 at atmospheric pressure per minute [20]. In 1968, Bergman introduced a prototype of a complete optical system that comprised all the components of the modern optical sensor, including a miniature UV emitting glow lamp, a UV transmitting filter, a fluoranthene disk, a UV absorbing filter, and a cadmium sulfide photoconductive cell responded to nitrogen [21].

Peterson et al. [22] proposed an oxygen flow visualization (imaging) technique by spraying and then imaging the oxygen stream on a silica gel thin-layer chromatography plate covered by absorbing dyes. They introduced this technique as a new method to study the oxygen flow over airfoil shapes or the behavior of fluidic devices [22].

A breakthrough was realized when the group of David Wilson reported a new phosphorescence lifetime technique for measuring oxygen tension in biological samples based on oxygen-dependent quenching of metalloporphyrin probes [23]. This technique can be thought of as the single-photon analog to 2PLM and serves as the foundation for it. The Wilson group and other groups used this technique to measure pO_2 in perfused tissues [24], tumors [25], single capillaries [26], and many other applications uncovering new details about how oxygen delivery and consumption occurs in vivo. Most of this work was performed before two-photon excitation techniques were widely available, however.

The theoretical basis for two-photon excitation was first presented about 90 years ago in 1931 by Maria Göppert-Mayer [27]. In her doctoral dissertation she rightly predicted the phenomenon of two-photon absorption, but it was not until 1990 that two-photon excited microscopy became a reality. Denk et al. [28] reported the seminal work on two-photon excited fluorescence for laser scanning microscopy (LSM) with ultrafast pulsed lasers and opened a new window for nonlinear microscopy in biological samples [28, 29]. In the mid-2000s, two-photon excitation was finally applied successfully to phosphorescence lifetime measurement of oxygen in vivo [30]. 2PLM benefits from the use of near-infrared (NIR) excitation

wavelengths for two-photon excitation, where optical scattering and absorption is reduced in biological samples. Use of this NIR "optical window" typically leads to reduced photodamage and higher depth of penetration compared to single-photon excitation at visible wavelengths [31]. The possibility of widespread use of 2PLM gained traction later in 2008 when Finikova et al. reported an antenna-core probe to address the very low two-photon absorption (2PA) cross sections in the early generations of oxygen probes built around Pt or Pd metalloporphyrins [32]. Their technique, which they called two-photon laser scanning microscopy, made it possible to reliably image microvasculature and tissue oxygenation with high spatial resolution in live animals. Today, researchers are still designing novel high-performance 2PA phosphorescent probes to broaden the range of possible biomedical applications [33].

The patent from the Webb group and the publication in the journal Science in 1990 provided the first proof to the biological community that multiphoton excitation microscopy was a viable option for the imaging of biological systems [28]. 2PLM, as a new branch of this technique, facilitates direct insight into the tissue microenvironment by mapping oxygenation. The application of 2PLM to biomedical imaging and sensing has resulted in many critical experimental findings, especially on the role of oxygen in several physiological and pathological conditions.

4.2 Fundamentals of 2PLM

Developing optical imaging techniques like 2PLM that feature high spatial resolution while providing quantitative information about key microenvironmental factors such as oxygen can provide answers to some of the most important and challenging biomedical questions. To effectively apply 2PLM for biological studies, however, it is crucial to understand the components, mechanisms, and recent instrumentation development enabling this method.

4.2.1 Molecular Underpinnings of Phosphorescence Quenching

When electronic excitation of a molecule occurs from the absorption of a photon, the energy can dissipate via several mechanisms (Fig. 4.1). For many luminophores used in biological samples, the electronic transition from the ground state (S_0) to the singlet excited state (S_1) can occur via one- or two-photon absorption (Fig. 4.1) [34]. Two-photon excitation occurs from the simultaneous absorption of two lower-energy, higher-frequency photons, with a combined energy that matches the S_0 to S_1 energy differential (Fig. 4.1) [35]. Upon excitation to S_1, energy can be immediately lost through non-radiative vibrational relaxation to the lowest mode of S_1. From S_1, two major deactivation pathways are possible that result in emission: fluorescence in which energy is released directly from S_1 in the form of a photon while the molecule returns to S_0, and phosphorescence in which the molecule undergoes intersystem

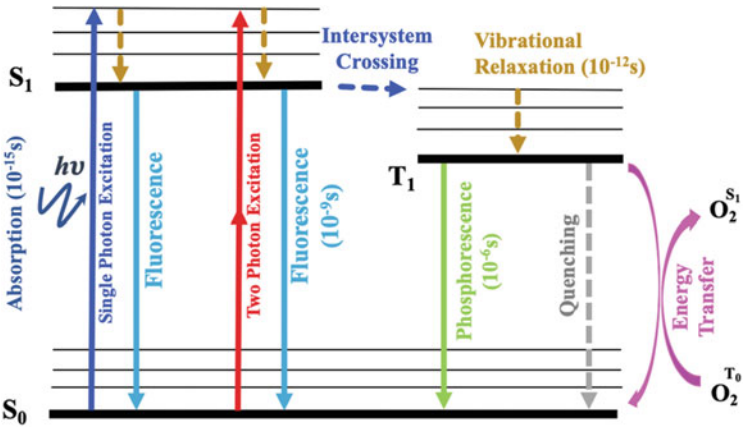

Fig. 4.1 Jablonski energy diagram highlighting some of the potential radiative and non-radiative deactivation pathways following light absorption by a model phosphor. Single-photon and two-photon excitation are shown as blue (UV-Visible wavelengths) and red (NIR wavelengths) arrows, respectively. Quenching of the triplet state (T_1) by bimolecular oxygen (O_2 T_0) results in the production of singlet oxygen (O_2 S_1) and the regeneration of the ground state phosphor (S_0)

crossing (via a change in electron spin from paired to unpaired) to the triplet excited state (T_1) before releasing energy in the form of a photon as the molecule returns to S_0 [34, 36]. Collisional quenching of T_1 by neighboring molecules or molecular structures can cause the T_1 to S_0 transition without emission of a photon. The effect of phosphorescence quenching by a single quencher [Q] results in a decrease in phosphorescence intensity and lifetime following the Stern–Volmer relationship:

$$I_0/I = \tau_0/\tau = 1 + K_q \times \tau_0 \times [Q], \tag{4.1}$$

where I_0 and τ_0 are the intensity and lifetime of phosphorescence emission in the absence of quencher, respectively, I and τ are the intensity and lifetime at a specific concentration of quencher [Q], respectively, and K_q is the quenching constant [37–39]. Bimolecular oxygen (O_2) is one of the most potent dynamic quenchers in physiologically relevant conditions resulting in very efficient quenching of most phosphors [19]. This dynamic quenching can be exploited to quantitatively measure pO_2 since the average lifetime of phosphorescent emission depends directly on the pO_2 in the environment surrounding an excited phosphor according to Eq. (4.1). When quenching occurs, energy is transferred from T_1 to triplet biomolecular oxygen converting it to highly reactive singlet oxygen (Fig. 4.1) [19, 40]. Singlet oxygen, as a by-product of the quenching process, and its derivatives (reactive oxygen species or ROS) are highly reactive molecules that can efficiently react with nearby biological molecules resulting in undesirable phototoxicity as a potential side-effect of 2PLM [34, 41]. Advantageously, the inherent two-photon absorption mechanism of 2PLM prevents singlet oxygen production outside of the focus, thereby minimizing the total singlet oxygen typically produced by several orders

of magnitude compared to single-photon phosphorescence lifetime microscopy. Nevertheless, singlet oxygen production via triplet state quenching can be used constructively as in the case of photodynamic therapy, a promising antitumor strategy in mainstream cancer treatment [42, 43].

4.2.2 Experimental Setup of 2PLM for Oxygen Sensing

Many of the modern 2PLM systems are composed of semi-independent imaging and sensing arms or sequentially acquired imaging and sensing modes that share the same optical path [33, 44–47]. The imaging mode provides the user with a way to visualize the area of interest based on fluorescence emission with a high frame rate. This fast imaging approach is beneficial for many in vivo experiments since the region of interest must be identified in a relatively short time (e.g., while the animal is under anesthesia). The sensing mode provides excitation/emission cycles for phosphorescence lifetime measurement typically on a pixel by pixel basis and is often very slow ($\sim 10^3$ to 10^6 slower) relative to the imaging mode [48–50]. This slow speed can be attributed to the difference in natural lifetimes of fluorescence (typically ~1–10 ns) and phosphorescence (typically ~1–100μs) and the low quantum yield of phosphorescence (often <0.1 at physiological oxygen tension) compared to fluorescence (often >0.2). The phosphorescence emission is typically too slow and too dim to be useful for image formation in intravital measurements.

For certain oxygen sensing probes (e.g., Pt meso-tetraarylporphyrin-coumarin-343 [PtP-C343]), two-photon absorption occurs via two-photon antenna chromophores embedded in the molecule that can then transfer the energy via fluorescence resonance energy transfer (FRET) to the core metalloporphyrin for oxygen quenching [32]. In this type of probe, the contrast for imaging and lifetime sensing can originate from the same molecule [32]. The drawback of such a dual-purpose probe is that the fluorescence emission overlaps with blue-green wavelengths often reserved for molecular reporters based on fluorescent proteins (e.g., CFP/GFP/YFP). We encountered this issue when using PtP-C343 for oxygen measurements in the bone marrow of knock-in mice with GFP-labeled endogenous hematopoietic stem cells (HSCs) [51]. The relatively weak GFP-HSC reporter was overshadowed by the strong fluorescence emission of the PtP-C343. We overcame this challenge by switching to a two-photon excitable probe (Pt-G4), generously provided by Dr. Sergei Vinogradov, that gave no detectable background fluorescence in the GFP emission band.

As observed in Fig. 4.2, 2PLM images are generated by *x-y* raster scanning of a femtosecond pulsed laser (e.g., titanium sapphire laser) using fast-scanning mirror combinations (e.g., polygon/galvanometer or dual galvanometer scanners) that provide lateral focal-point positioning. Dichroic mirrors (for cases where the imaging excitation wavelength and lifetime measurement excitation wavelength are different) and polarizing beam splitters are commonly used for splitting and/or combining the imaging and sensing arms of a 2PLM system (Fig. 4.2). Phosphorescence lifetime measurements are typically acquired in the time domain whereby an excitation gate

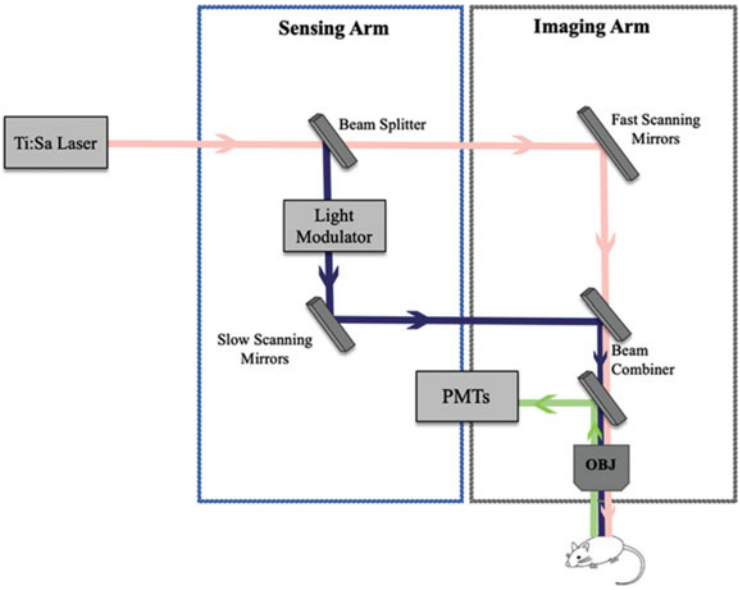

Fig. 4.2 Generalized microscope setup for 2PLM. For imaging, light from a Titanium Sapphire laser (Ti:Sa) is scanned by fast-scanning mirrors and focused onto the sample by an objective lens (Obj). For phosphorescence sensing, the light is gated by a light modulator and directed by a slow-scanning mirror through the objective lens onto the sample. The fluorescence is collected by a standard photo-multiplier tube (PMT) while the phosphorescence is captured by a photon-counting PMT module to be saved for later processing

consisting of tens to hundreds of individual laser pulses is created by passing the laser through an electro-optic modulator (EOM) or an acoustic-optic modulator (AOM). The modulated beam is directed laterally by slow-scanning mirrors and focused by an objective lens to excite the sample. The resulting phosphorescence emission decay is collected by a very sensitive detector (usually a photon-counting Photo-Multiplier Tube [PMT]) and synchronized to the excitation gate so that the photon arrival times can be measured relative to the excitation gate. Due to very low signal, hundreds to sometimes thousands of excitation/emission cycles are collected for each focal point in the sample, and a histogram of arrival times is generated until an acceptable (~20–25) signal-to-noise ratio (SNR) is achieved [32]. To determine the phosphorescence lifetime, the phosphorescence intensity decay histogram is fitted with an exponential decay function to calculate the phosphorescence lifetime. This lifetime is then compared against a calibration plot obtained from independent in vitro oxygen titration experiments to convert the lifetime value to pO_2 [32].

For a relatively low-light level technique such as 2PLM, considerations need to be made about how to handle the collected photon signal in a manner that maximizes SNR. This is especially important when considering that the accuracy of the calculated lifetime (and subsequent measurement of oxygen tension) is directly dependent on the SNR of the collected signal. The most common method of choice

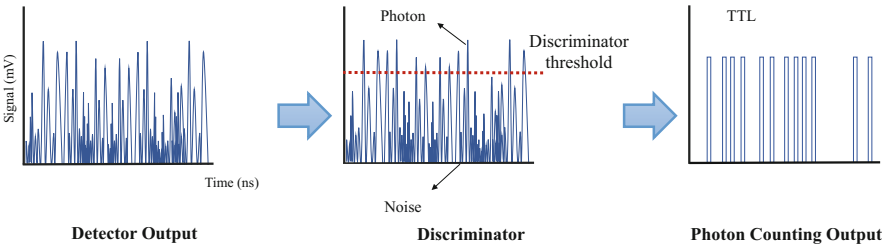

Fig. 4.3 Single-Photon Counting (SPC) diagram. The raw detector electronic output is filtered by a discriminator that rejects electronic peaks below an empirically defined threshold and converts peaks above the threshold to individual TTL outputs for recording by a computer

in 2PLM is single-photon counting (SPC). SPC can refer to several different techniques that have in common the goal of recognizing true photonic signal while rejecting electronic noise [52, 53]. Conceptually, SPC can be thought of as an electronic filtering technique based on an empirically defined threshold (Fig. 4.3). PMTs used for 2PLM are capable of detecting a single photon but they suffer from significant dark current (or dark counts) from the dynode amplification process. SPC enables much of this noise to be filtered out since noise peaks originating from dynodes within the PMT are typically weaker than what is generated by a photon striking the photocathode. In SPC, the raw detector output is filtered through a discriminator with an adjustable threshold that is preselected empirically based on the peak SNR of the specific detector (Fig. 4.3) [52]. Electronic peaks above the threshold are considered "true" photon peaks and are digitized with transistor-transistor logic (TTL) (or similar digital logic with high noise immunity) and recorded by a computer with a data acquisition card. Any peaks below the threshold are rejected which includes most of the dark current (Fig. 4.3). SPC does not reject background signal from ambient light or endogenous luminescence of the sample, so care should be taken in eliminating signal from those sources separately.

4.2.3 Improvements for 2PLM

4.2.3.1 Time Acquisition and Lifetime Improvement

Although 2PLM systems have brought a lot of benefits for oxygen sensing in tissue, due to long triplet lifetimes and low photon count rates relative to 2-photon excited fluorescence, the temporal function of conventional 2PLMs is limited, especially when considering fast-moving cells (e.g., activated T cells) or motion artifacts (e.g., breathing and heart beat) in live animals [54]. In principle, frame rates in phosphorescence lifetime microscopy can be enhanced by implementing gated cameras, or frequency-domain spatial multiplexing, although these techniques can suffer from poor depth resolution [55, 56]. S. S. Howard et al. [56] experimentally demonstrated a parallel-excitation/parallel-collection MPM–PLIM system [56]. In their adaptive optics system, multiphoton laser scanning microscopy was integrated with custom

reflection-based spatial light modulators as an adaptive beam shaping technique to form a linear array of point sources that are modulated by different frequencies [56]. They reported that in comparison with conventional configurations, the designed microscopy improves the pixel rate by 100 times while simultaneously acquiring intensity images and phosphorescence lifetime at depth [56]. In 2019, M. Rytelewski et al. developed a "Fast" Scanning Two-photon Phosphorescence Lifetime Imaging Microscope (FaST-PLIM) that differs from the conventional 2PLM in the signal accumulation approach and also unitary acquisition design [54]. Each pixel in FaST-PLIM receives only one excitation/emission cycle gate before the next pixel is excited. They decreased the decay measurement period for each cycle since full recovery of the phosphor to ground state is not required for accurate measurement with this unitary acquisition regime. With this increased acquisition speed, they succeeded to directly observe and investigate the relationship between fast-moving T-lymphocytes and local oxygen concentration in tumors [54]. They found that T-lymphocyte motility was significantly decreased in regions of hypoxia within the mouse bone marrow [54].

4.2.3.2 Saturation Effects

In two-photon excited microscopy, the probability of TPA depends on the square of the excitation intensity and is limited to the diffraction limited focal volume [57]. At very high excitation intensities, however, due to saturation effects of the excited state the quadratic dependence is lost. When this occurs, a fraction of neighboring molecules outside of the laser focus enter S_1, expanding the excitation volume and thus degrading the resolution and efficiency of excitation [58]. For biomedical researchers using fluorescence microscopy, saturation effects are rarely observed since high excitation powers are usually avoided due to negative biological effects.

When considering two-photon excited phosphorescence, however, saturation is common since the lifetime of T_1 can be $>10^4$ times longer lived than S_1. Each subsequent pulse of an ultrafast optical oscillator (e.g., Ti:Sa laser) operating at 80 MHz repetition rate can pump an increasing number of S_0 molecules into the T_1 state before a significant fraction of them can relax to S_0 resulting in a population inversion. When saturation occurs, the efficiency of each subsequent laser pulses decreases, and the spatial resolution of the measurement degrades. In order to obtain a detectable phosphorescent signal, working in the saturation regime is often unavoidable for in vivo 2PLM. Popular metalloporphyrin probes used for 2PLM are known to have very low two-photon absorption cross sections and very low quantum yields of phosphorescence [59].

One obvious solution to avoid saturation effects is to minimize the average excitation power. A multiple foci approach can be employed, where power is distributed over several foci to minimize the saturation effects of any individual focal volume [60]. Another option to minimize saturation effects is focus shaping. We previously employed a focus shaping technique where the laser beam was scanned across a 100μm slit that was conjugated to the focus in the sample (Fig. 4.4a) [44]. This elegant technique generates an excitation gate while also scanning the focused beam in the sample by a few micrometers laterally during

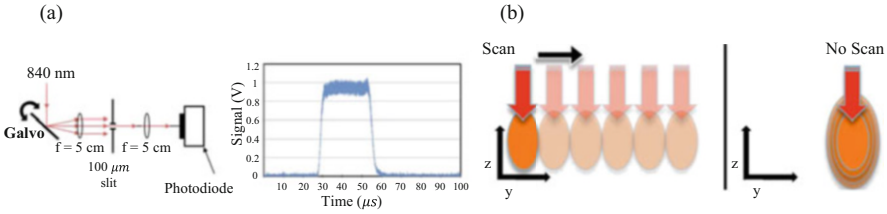

Fig. 4.4 (**a**) Schematic setup of the scanned slit and its excitation pulse graph indicating how the galvanometer scans the focused beam across a slit to form the excitation gate. In experiment mode, the photodiode is removed so that the light can pass through the rest of the system to illuminate the sample (not shown). (**b**) Comparison of scanning across a slit vs. a stationary focused beam. The focal volume increases and resolution decreases with each subsequent excitation pulse during the excitation gate [61]

the ~10–40μm excitation gate (Fig. 4.4a) [44, 61]. Unlike stationary beams which increase the focal volume and decrease resolution (especially in the *z*-axis) with each subsequent laser pulse of the excitation gate, scanning across a slit minimizes saturation effects, leading to more efficient use of laser power and better retention of axial resolution (Fig. 4.4b).

4.2.3.3 Phosphorescent Probe Design

Optimizing the phosphorescent probe design by selecting molecules with a high quantum yield of phosphorescence and a strong 2PA cross section are key to improving the SNR in 2PLM and increasing the acquisition speed [62]. To date, metalloporphyrin molecules have been considered as the best phosphorescent oxygen sensitive probes [32, 63]. What distinguishes these molecules from other probes is their high sensitivity to the physiological range of pO_2, high stability at room temperature or 37 °C, their potential to be chemically modified to diminish the effect of external factors like pH or protein binding, and above all, relatively good phosphorescent quantum yields [63–65]. Originally, three main groups of metalloporphyrins were created for phosphorescence lifetime measurement: unmodified metalloporphyrins, polyglutamate dendrimer metalloporphyrins, and polyarylglycine dendrimer metalloporphyrins surrounded by long polyethylene glycol (PEG) residues [64, 65]. One of the main limitations of the first two groups is the dependency on albumin binding for sensitivity in the physiological range of pO_2. Since the albumin concentration is ~600μM in blood, some fraction of molecules remain unbound making the interpretation inaccurate and unreliable [63–66]. Decoration of the third generation of probes with PEG prevents binding to biological molecules such as albumin, thereby making them more reliable even in the presence of biomacromolecules [32, 63]. Furthermore, the lack of binding to biomolecules makes them good candidates for extravascular measurement if they can be delivered to the interstitial space [65]. Most oxygen sensor probes synthesized since then have been designed with a similar architecture to the third-generation probes. Among proposed oxygen probes [67], PtP-C343 was the first practical two-photon absorbing oxygen probe to have been widely applied in different biological applications

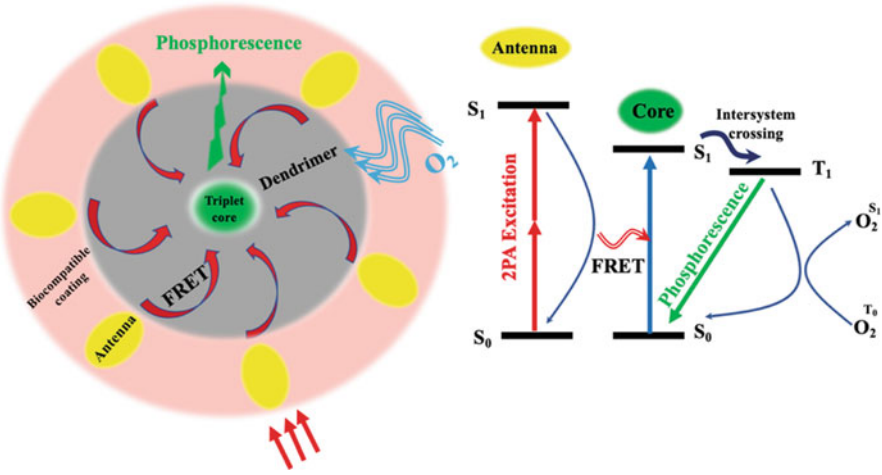

Fig. 4.5 Schematic and energy diagram of 2PA antennae probes. Two-photon energy (Red arrows) is absorbed by several 2P-antenna chromophores (Yellow ovals) and transferred to the metalloporphyrin-core (Green oval) via FRET. When the excited phosphorescent probes are exposed to oxygen (Blue arrow), energy from the triplet state (T_1) is quenched by triplet oxygen

[44, 45, 59]. Due to the very low two-photon absorption cross section of the core metalloporphyrin, PtP-C343 relies on coumarin-343 moieties to act as two-photon antennae that transfer the absorbed energy to the core metalloporphyrin via FRET [32]. The generalized schematic of 2PA antennae oxygen probes like PtP-C343 is shown in Fig. 4.5 [24].

2PA antennae probes have complex chemical structures and require strict fine tuning of the distance between the antenna chromophores and the core porphyrin. Small deviation in the distance can significantly reduce the probe's emissivity and degrade imaging performance. Recently, scientists in the group of Dr. Sergei Vinogradov reported Oxyphor 2P as a new direct two-photon excitable oxygen probe. The single chromophore has intrinsically high quantum yield and 2PA cross section rendering it 50–60 times brighter than previous metalloporphyrin oxygen sensors [30]. Because Oxyphor 2P is not an antennae probe, it overcomes limitations associated with core-antenna 2PA probes. Breakthroughs in design, such as the 50–60× increase in signal, open up new possibilities for faster oxygen sensing techniques and potentially 3D oxygen mapping at a reasonable frame rate [33].

4.3 Oxygen Measurement by 2PLM

In humans, the brain is responsible for ~25% and 20% of the glucose-derived energy consumption and net oxygen consumption, respectively, while it comprises just 2% of the body weight [68]. Providing a sufficient oxygen supply through a highly specialized vascular system is essential for maintenance of healthy brain function.

Table 4.1 An overview of in vivo 2PLM pO_2 measurements

Probe location	Probe name	Application	References
Brain of anesthetized animals	PtP-C343	Mapping of pO_2 in blood vessels and tissue at steady state and during various stimulations or occlusions to understand oxygen delivery and consumption.	[32, 45, 59, 72–77]
	Oxyphor 2P	Synthesis of Oxyphor 2P as a new 2PA probe for cortical oxygen measurement	[33]
Brain of awake animals	PtP-C343, Oxyphor 2P	Mapping of pO_2 in awake animals to study brain oxygenation within the cortex.	[46, 47, 78–82]
Bone marrow	PtP-C343, PtTCHP-C307, Pt-G4	Direct in vivo measurements of pO_2 in the bone marrow and hematopoietic stem cell niche in normal and diseased states.	[44, 54, 55, 67, 83]
Retina	Pt(II) tetra phthalimidoporphyrin	In vivo depth-resolved imaging of pO_2 in the retinal capillary plexus.	[84]
Tumor (Bone marrow)	PtP-C343	FaST-PLIM system to investigate the dependency of T-lymphocyte motility on oxygen distribution in tumors.	[54, 83]

Today a growing list of human disorders including Alzheimer's disease (AD) [69], Parkinson's disease (PD) [70], and Huntington's disease (HD) [71] are found to be associated with deficiencies in tissue oxygen or cerebrovascular dysfunctions. For this reason, there has been an increased focus on studying the dynamics of cerebral oxygen delivery and consumption to better understand the role that oxygen plays in normal and diseased states of the brain.

The introduction of PtP-C343 as the first practical two-photon phosphorescent nanoprobe by the Vinogradov team in 2008 serves as a milestone for oxygen mapping via 2PLM and has led to an interest in applying 2PLM to understand the fundamental role of oxygen in a variety of tissues and contexts in vivo (Table 4.1) [32]. PtP-C343 provides a significant improvement over previous probes in terms of 2PA cross section, measurement depth in tissue, and the minimization of singlet oxygen production [30]. Using PtP-C343 for the first time, Finikova et al. reported a combination of phosphorescence quenching with two-photon laser scanning microscopy (2PLSM) that enable them to record high-resolution images of oxygen distributions in heterogeneously oxygenated glass pipettes and cells [32]. Following PtP-C343 synthesis, Sakadzic et al. used the 2PLM technique to demonstrate in vivo two-photon pO_2 measurements with high resolution, depth of penetration up to 250μm, and low probe concentration in living rodent cortical tissue and microvasculature [59].

In 2011, Devor et al. reported the dependence of cerebral tissue oxygen changes on the baseline pO_2 level and stimulus duration when evoked by sensory stimulation. They found that in tissue sites that are at the low baseline pO_2, constant stimulation

won't overshoot the oxygen tension from the baseline to a high pO_2 level. In contrast, during stimulus-evoked activation, transient decreases occur during the "initial dip" and "poststimulus undershoot." Their results suggest the elevated pO_2 in blood during the hemodynamic response functions to maintain the oxygen tension at normal levels for tissue sites far from the blood vessels [72]. Parpaleix et al. [73] then showed the initial dip in pO_2 at the level of capillaries during odor stimulation and reported that oxygen dynamics in cerebral capillaries reflects neuronal activity. They also investigated the range to which erythrocyte-associated transients (EATs) reflect the neuronal activity. Based on their results, at rest the pO_2 between two EAT is closer to the real physiological pO_2 in the neuropil relative to reported pO_2 from EAT peaks [73]. In another related experiment, the Lecoq group [74] mapped oxygen in various vascular compartments and showed the existence of diffusion-based arterio-venous shunts. Their study also showed that at the site of synaptic transmission, odor evokes a pO_2 increase in vasculature which is preceded by an initial dip in the neuropil [74].

Sakadžić et al. [75] incorporated a two-photon microscopy (TPM) and Doppler optical coherence tomography (OCT) imaging setup and demonstrated that precapillary arterioles and low-branching-order capillaries are responsible for supplying most of the oxygen to the cortical tissue at baseline, while high-branching-order capillaries serve as a buffer to secure enough oxygen, especially during high oxygen consumption or low blood flow conditions [75]. The results of their study provide valuable information for the interpretation of fMRI data and may help inform the development of improved fMRI techniques. In another project, using TPM and Doppler OCT, Moeini et al. (2020) quantified the cerebral pO_2 and blood flow in awake mice during forced treadmill exercise to investigate the relationship between cerebral tissue oxygenation, capillary flow, and exercise intensity. Their study showed that compared to rest, cerebral pO_2 and perfusion increase during running at 5 m/min. At faster speeds (10 and 15 m/min), however, arteriolar and capillary blood flow decreases while tissue oxygenation remains unchanged likely due to autoregulation and an increase in RBC linear density [81].

Using 2PLM, Sakadžić et al. [45] succeeded to map the periarteriolar tissue pO_2 in the brain and fit the changes of oxygen tension with the Krogh cylinder model of oxygen diffusion to estimate the cerebral metabolic rate of oxygen ($CMRO_2$) [45]. Estimation of $CMRO_2$ is a valuable but challenging task that requires complex multimodal imaging and mathematical modeling. $CMRO_2$ interpretations are used for analysis of brain function and diagnosis of cortical pathological conditions, so the invention of new approaches for simplifying its calculations may lead to a better understanding of the metabolic rate of oxygen in the brain under various conditions.

Lyons et al. [78] used awake mice to study the cortical oxygenation with 2PLM and PtP-C343. They reported that isoflurane enhances the capillary RBC flow and thus leads to positive error in brain oxygenation measurements. To reduce the anesthetic effect, they studied the cerebral pO_2 for the first time in an unstressed, awake mouse through a cranial window and reported accurate values of pO_2 close to the physiological conditions in the vasculature and interstitium of mouse cerebral grey matter. Since accurate measurement of the oxygen tension is critical for

investigating neural interactions and diseases associated with them, their work can provide standard values for other researchers to investigate neural processes and model brain metabolism [78]. The same group also reported that imaging through a cranial window with a water immersion objective at room temperature lowers the brain temperature, decreases cerebral blood flow, and can invalidate pO_2 measurements based on phosphorescence lifetime. They demonstrated that although postsurgical decrease of brain temperature returns to normal after a couple of days, imaging with a water immersion objective reduces the temperature again by 2–3 °C. To eliminate this effect, they found that a dry objective or heated water immersion objective can diminish the temperature fluctuation and produced more accurate results [79]. In aged awake mice, Moeini et al. [46] studied age-associated alternations in brain oxygenation within the barrel cortex. Using awake mice was key for this experiment since anesthesia might affect physiological and hemodynamic parameters correlated with aging leading to a false interpretation of the results. They reported that aging is accompanied by lower pO_2 in cerebral arterioles and venules, lower cerebral tissue pO_2, and more spatial heterogeneities in the distribution of oxygen in tissue. The detection of hypoxic micro-pockets and a significant decrease in brain oxygenation with aging is an important finding that has important implications for neurodegenerative diseases and cognition decline in elderly people [46].

Kazmi et al. [76] designed an experiment in which they mapped changes in intravascular oxygen tension of the brain before and after occlusion by exploiting real-time Laser Speckle Contrast Imaging (LSCI) to guide the occlusion process and 2PLM techniques to measure the pO_2. This study helped to underline the role of vascular networking on pre- and post-occlusion oxygenation [76].

Using 2PLM, K. Kisler et al. [77] confirmed the key role of pericytes in the regulation of cerebral blood flow (CBF) in response to stimuli [77]. They reported that in pericyte-deficient mice, following neuronal stimuli there was a decrease in CBF that, in turn, caused neurovascular uncoupling and reduced oxygen supply to the brain. Given that pericytes are degraded in Alzheimer's disease, knowing the mechanism for how the dysfunction of these cells affects the brain may help lead to the development of better diagnosis and treatment of neurologic disorders.

On a different note, Q. Zhang et al. [80] took advantage of polarography, spectroscopy, and 2PLM techniques to measure oxygen levels in the cortex of awake mice during locomotion and found that locomotion considerably enhances brain oxygenation, specifically in the olfactory bulb, frontal cortex sites and regions that are more engaged in locomotion [80].

Recently, significant progress was made on probe design for 2PLM oxygen sensing. In 2019, Esipova et al. [33] introduced a new two-photon oxygen probe, Oxyphor 2P, with 50–60 times brighter signal than all previous metalloporphyrin probes used for oxygen sensing. To validate its performance for longitudinal measurement and quantitative imaging of pathological states, they measured tissue oxygenation for 4 days after induction of a single-capillary micro-stroke in the cortex [33]. Due to its high signal, Oxyphor 2P has the potential of being employed with 2PLM to determine the tissue metabolic states in a variety of biomedical

contexts. In 2020, Kritchenkov et al. synthesized new oxygen probes based on iridium (Ir) complexes with high quantum yields around 13–15%. They found these probes had relatively short lifetimes in the range of 1–2.5 μs which is advantageous for fast data acquisition during real-time oxygen sensing [85]. Combining advances in applying 2PLM to awake animals with the advances in Oxyphor 2P synthesis, Li et al. [47] measured the absolute intravascular pO_2 in an large number of arterioles, venules, and capillaries (6544 vascular segments vs. <100 capillaries in Lyons et al. study), as well as RBC-pO_2, InterRBC-pO_2, EAT, and RBC flow properties in capillaries across layers I–V (Max depth 600 mm vs. ~410 mm from Lyons et al. [78]). Their results revealed that the intracapillary resistance to oxygen delivery, the RBC flux, and oxygenation heterogeneity are higher in upper cortical layers compared to the deeper regions while in Layer IV, where oxygen consumption is the maximum, the oxygen extraction fraction is enhanced [47]. These detailed findings provide deep insights into layer-dependent oxygen delivery and consumption in the brain. Consistent with this study, Sencan et al. (2020) used Oxyphor 2P to show that in response to sensory stimulation, alterations in intravascular pO_2 are conserved across cortical layers I–IV. In contrast to the previous reports performed in anesthetized animals they showed that there is no "initial dip" of intravascular oxygen tension in awake mice following sensory stimulation. In addition, they found O_2 saturation increases more in the venules compared to arteries [82].

While 2PLM oxygen sensing in the brain is an extremely important avenue of investigation, there remains significant opportunities for applying 2PLM to understand the role of oxygen in other biological contexts. For example, we performed the first direct in vivo measurements of local oxygen tension in the bone marrow and hematopoietic stem cell niche of live mice using PtP-C343 and Pt-G4 [44, 51]. We uncovered heterogeneities in local pO_2, with the lowest pO_2 found in deeper perisinusoidal regions and less hypoxic areas closer to the endosteal region [44]. We found that endogenous hematopoietic stem and progenitor cells do not reside in the most hypoxic regions of the bone marrow at steady state [51]. When the bone marrow was altered by radiation and chemotherapy, however, we discovered a significant increase in pO_2, pointing to the role of stress in altering the stem cell metabolic microenvironment [44].

In collaboration with the Vinogradov lab in 2014, we presented a new probe, PtTCHP-C307, which was designed to overcome limitations of PtP-C343 by providing improvements in phosphorescence quantum yield, efficiency of the antenna-core energy transfer, improved signal dynamic range, and minimized quenching of the phosphorescence by electron transfer [67]. PtTCHP-C307 performance was validated in vivo by acquiring pO_2 measurement through the intact mouse skull into the bone marrow as previously described but with minor improvement in signal intensity [44, 67]. In another bone marrow study, Rytelewski et al. [54] developed a novel imaging regimen (FaST-PLIM) which is able to map tissue oxygenation in vivo at cellular resolution while enabling the capture of cellular dynamics. In this study they established FaST-PLIM to directly visualize the relationship between local oxygen concentrations and T-lymphocyte (T cell) motility in

tumors and found the motility of T cells depends on the local oxygen concentration. This study introduced the FaST-PLIM system as a potentially valuable tool for oxygen sensing in a wide range of biological studies where acquisition time is important [54]. In 2020, using this new optical system they studied extracellular oxygen concentrations in a model of leukemia. They used intracellular hypoxia measurement with pimonidazole in combination with 2PLM to couple the extracellular oxygen levels to intracellular hypoxia at different stages of the B-cell acute lymphocytic leukemia (B-ALL). They discovered that during the initial and intermediate disease stages due to expansion of vascular network, pO_2 increases externally while intracellular hypoxic is still present. In end stage disease, they observed that high cellularity and metabolic demands of the tumor cells led to increased intracellular hypoxia and a shift in the external hyperoxia to a noticeable pO_2 reduction [83].

2PLM oxygen sensing has also been applied in other contexts. For example, Schilling et al. [86] developed an implantable polymeric mesh including PtP-C343 which was capable of supporting bone marrow stromal cell growth and differentiation. Designed electrospun fibers were applied to report oxygen levels with high spatial resolution during bone regeneration in real time. Their new carriage system for probe delivery showed promise for overcoming the common limitations like accumulation in the interstitial space over time due to leaky vasculature or the lack of distribution in tissues that have not yet been vascularized [86]. 2PLM oxygen sensing has also been applied for the first time to the retina in vivo. Sencan et al. [84] reported absolute pO_2 measurements in the superficial, intermediate, and deep retinal microvascular plexus under both normoxia and hyperoxia [84]. The authors hope that implementing 2PLM for pO_2 measurement in retinal microvasculature will lay a foundation for additional studies on the physiology of retinal disorders.

4.4 Conclusion

2-photon phosphorescence lifetime microscopy (2PLM), as a robust nonlinear optical microscopy technique, has received a lot of attention recently due to its potential for quantitative pO_2 imaging in tissue with high spatial resolution. In this chapter, we provided background on the development of 2PLM, discussed the most common oxygen sensing measurement methods and concepts, and explained the general principles and optical configurations of a 2PLM system. We discussed the key characteristics and strategies for improvement of the technique and presented an overview of how 2PLM has been used for oxygen sensing in biological applications to improve our understanding of the basic biology underlying several areas of human health.

2PLM has the potential to help answer some of the most challenging and important questions related to the role of oxygen in biology and medicine. Even though 2PLM has become the premier tool for studying oxygen in vivo, it is still relegated to a small subset of specialists due to the cost and expertise required to build a 2PLM system and the expertise required to synthesize the phosphor probes.

Therefore, significant hurdles remain to the widespread availability of this technique for the broader scientific community. Nevertheless, with new developments in both the instrumentation and the phosphor probe design, there is hope that even these hurdles will be overcome.

References

1. Chelushkin PS, Tunik SP (2019) Phosphorescence lifetime imaging (PLIM): state of the art and perspectives. In: Yamanouchi K, Tunik S, Makarov V (eds) Progress in photon science, vol 119. Springer International Publishing, Cham, pp 109–128
2. Shcheslavskiy I, Neubauer A, Bukowiecki R, Dinter F, Becker W (2016) Combined fluorescence and phosphorescence lifetime imaging. Appl Phys Lett 108(9):091111. https://doi.org/10.1063/1.4943265
3. McGown LB, Nithipatikom K (2000) Molecular fluorescence and phosphorescence. Appl Spectrosc Rev 35(4):353–393. https://doi.org/10.1081/ASR-100101229
4. Yamanouchi K, Tunik S, Makarov V (eds) (2019) Progress in photon science: recent advances, vol 119. Springer International Publishing, Cham
5. Clerici WJ, Hensley K, DiMartino DL, Butterfield DA (1996) Direct detection of ototoxicant-induced reactive oxygen species generation in cochlear explants. Hear Res 98(1–2):116–124. https://doi.org/10.1016/0378-5955(96)00075-5.
6. Kizaka-Kondoh S, Konse-Nagasawa H (2009) Significance of nitroimidazole compounds and hypoxia-inducible factor-1 for imaging tumor hypoxia. Cancer Sci 100(8):1366–1373. https://doi.org/10.1111/j.1349-7006.2009.01195.x
7. Papkovsky DB (2004) Methods in optical oxygen sensing: protocols and critical analyses. In: Methods in enzymology, vol 381. Elsevier, Amsterdam, pp 715–735
8. Swartz HM, Walczak T (1998) Developing in vivo EPR oximetry for clinical use. In: Hudetz AG, Bruley DF (eds) Oxygen transport to tissue XX, vol 454. Springer, Boston, MA, pp 243–252
9. International Society on Oxygen Transport to Tissue, Takahashi E, Bruley DF (2010) Oxygen transport to tissue XXXI. Springer, New York, NY
10. Swartz HM et al (2004) Clinical applications of EPR: overview and perspectives. NMR Biomed 17(5):335–351. https://doi.org/10.1002/nbm.911.
11. Swartz HM et al (2014) Clinical EPR. Acad Radiol 21(2):197–206. https://doi.org/10.1016/j.acra.2013.10.011.
12. Schafer R, Gmitro AF (2015) Dynamic oxygenation measurements using a phosphorescent coating within a mammary window chamber mouse model. Biomed Opt Express 6(2):639. https://doi.org/10.1364/BOE.6.000639.
13. Raleigh JA, Chou S-C, Arteel GE, Horsman MR (1999) Comparisons among pimonidazole binding, oxygen electrode measurements, and radiation response in C3H mouse tumors. Radiat Res 151(5):580. https://doi.org/10.2307/3580034.
14. Chitneni SK, Palmer GM, Zalutsky MR, Dewhirst MW (Feb. 2011) Molecular imaging of hypoxia. J Nucl Med 52(2):165–168. https://doi.org/10.2967/jnumed.110.075663
15. Clark LC, Wolf R, Granger D, Taylor Z (Sep. 1953) Continuous recording of blood oxygen tensions by polarography. J Appl Physiol 6(3):189–193. https://doi.org/10.1152/jappl.1953.6.3.189
16. Niazi A (2016) Real time measurement of oxygen by integrating a clark sensor with low cost printed circuit board technology and solid electrolyte membrane. University of Birmingham, Birmingham, p 138
17. Shell JR, LaRochelle EP, Bruza P, Gunn JR, Jarvis LA, Gladstone DJ (2019) Comparison of phosphorescent agents for noninvasive sensing of tumor oxygenation via Cherenkov-excited luminescence imaging. J Biomed Opt 24(03):1. https://doi.org/10.1117/1.JBO.24.3.036001.

18. Wolfbeis OS (2015) Luminescent sensing and imaging of oxygen: fierce competition to the Clark electrode. BioEssays 37(8):921–928. https://doi.org/10.1002/bies.201500002
19. Kautsky H (1939) Quenching of luminescence by oxygen. Trans Faraday Soc 35:216. https://doi.org/10.1039/tf9393500216
20. Pollack M, Pringsheim P, Terwoord D (1944) A method for determining small quantities of oxygen. J Chem Phys 12(7):295–299. https://doi.org/10.1063/1.1723942
21. Bergman I (1968) Rapid-response Atmospheric oxygen monitor based on fluorescence quenching. Nature 218(5139):396–396. https://doi.org/10.1038/218396a0
22. Peterson JI, Fitzgerald RV (1980) New technique of surface flow visualization based on oxygen quenching of fluorescence. Rev Sci Instrum 51(5):670–671. https://doi.org/10.1063/1.1136277
23. Vanderkooi JM, Wilson DF (1986) A new method for measuring oxygen concentration in biological systems. In: Longmuir IS (ed) Oxygen transport to tissue VIII, vol 200. Springer, Boston, MA, pp 189–193
24. Rumsey WL, Vanderkooi JM, Wilson DF (1988) Imaging of phosphorescence: a novel method for measuring oxygen distribution in perfused tissue. Sci New Ser 241(4873):1649–1651
25. Dewhirst MW et al (1999) Quantification of longitudinal tissue pO2 gradients in window chamber tumours: impact on tumour hypoxia. Br J Cancer 79(11–12):1717–1722. https://doi.org/10.1038/sj.bjc.6690273.
26. Zheng L, Golub AS, Pittman RN (1996) Determination of PO2 and its heterogeneity in single capillaries. Am J Physiol Heart Circ Physiol 271(1):H365–H372. https://doi.org/10.1152/ajpheart.1996.271.1.H365
27. Göppert-Mayer M (1931) Über Elementarakte mit zwei Quantensprüngen. Ann Phys 401 (3):273–294. https://doi.org/10.1002/andp.19314010303
28. Denk W, Strickler J, Webb W (1990) Two-photon laser scanning fluorescence microscopy. Science 248(4951):73–76. https://doi.org/10.1126/science.2321027
29. So PTC, Dong CY, Masters BR, Berland KM (2000) Two-photon excitation fluorescence microscopy. Annu Rev Biomed Eng 2:399
30. Estrada AD, Ponticorvo A, Ford TN, Dunn AK (2008) Microvascular oxygen quantification using two-photon microscopy. Opt Lett 33(10):1038. https://doi.org/10.1364/OL.33.001038.
31. Briñas RP, Troxler T, Hochstrasser RM, Vinogradov SA (2005) Phosphorescent oxygen sensor with dendritic protection and two-photon absorbing antenna. J Am Chem Soc 127 (33):11851–11862. https://doi.org/10.1021/ja052947c
32. Finikova OS et al (2008) Oxygen microscopy by two-photon-excited phosphorescence. ChemPhysChem 9(12):1673–1679. https://doi.org/10.1002/cphc.200800296
33. Esipova TV, Barrett MJP, Erlebach E, Masunov AE, Weber B, Vinogradov SA (2019) Oxyphor 2P: a high-performance probe for deep-tissue longitudinal oxygen imaging. Cell Metab 29 (3):736–744.e7. https://doi.org/10.1016/j.cmet.2018.12.022
34. Lichtman JW, Conchello J-A (2005) Fluorescence microscopy. Nat Methods 2(12):910–919. https://doi.org/10.1038/nmeth817
35. Terenziani F, Katan C, Badaeva E, Tretiak S, Blanchard-Desce M (2008) Enhanced two-photon absorption of organic chromophores: theoretical and experimental assessments. Adv Mater 20 (24):4641–4678. https://doi.org/10.1002/adma.200800402
36. Jaffe HH, Miller AL (1966) The fates of electronic excitation energy. J Chem Educ 43(9):469. https://doi.org/10.1021/ed043p469.
37. Evale BG, Hanagodimath SM (2010) Static and dynamic quenching of biologically active coumarin derivative by aniline in benzene–acetonitrile mixtures. J Lumin 130(8):1330–1337. https://doi.org/10.1016/j.jlumin.2010.03.011.
38. Laws WR, Contino PB (1992) [21] Fluorescence quenching studies: analysis of nonlinear Stern-Volmer data. In: Methods in enzymology, vol 210. Elsevier, Amsterdam, pp 448–463
39. Fraiji LK, Hayes DM, Werner TC (1992) Static and dynamic fluorescence quenching experiments for the physical chemistry laboratory. J Chem Educ 69(5):424. https://doi.org/10.1021/ed069p424.

40. Quaranta M, Borisov SM, Klimant I (2012) Indicators for optical oxygen sensors. Bioanal Rev 4(2–4):115–157. https://doi.org/10.1007/s12566-012-0032-y
41. Schweitzer C, Schmidt R (2003) Physical mechanisms of generation and deactivation of singlet oxygen. Chem Rev 103(5):1685–1758. https://doi.org/10.1021/cr010371d
42. Agostinis P et al (2011) Photodynamic therapy of cancer: an update. CA Cancer J Clin 61 (4):250–281. https://doi.org/10.3322/caac.20114
43. Ho AH-P (2017) Handbook of photonics for biomedical engineering, 1st edn. Springer, New York, NY
44. Spencer JA et al (2014) Direct measurement of local oxygen concentration in the bone marrow of live animals. Nature 508(7495):269–273. https://doi.org/10.1038/nature13034.
45. Sakadžic S et al (2016) Two-photon microscopy measurement of cerebral metabolic rate of oxygen using periarteriolar oxygen concentration gradients. Neurophotonics 3(4):045005. https://doi.org/10.1117/1.NPh.3.4.045005.
46. Moeini M et al (2018) Compromised microvascular oxygen delivery increases brain tissue vulnerability with age. Sci Rep 8(1):8219. https://doi.org/10.1038/s41598-018-26543-w.
47. Li B et al (2019) More homogeneous capillary flow and oxygenation in deeper cortical layers correlate with increased oxygen extraction. elife 8:e42299. https://doi.org/10.7554/eLife.42299
48. Redondo CS et al (2017) Interplay of fluorescence and phosphorescence in organic biluminescent emitters. J Phys Chem C 121(27):14946
49. Baggaley E, Weinstein JA, Williams JAG (2014) Time-resolved emission imaging microscopy using phosphorescent metal complexes: taking FLIM and PLIM to new lengths. In: Lo KK-W (ed) Luminescent and photoactive transition metal complexes as biomolecular probes and cellular reagents, vol 165. Springer, Berlin, pp 205–256
50. Choi H et al (2012) 3D-resolved fluorescence and phosphorescence lifetime imaging using temporal focusing wide-field two-photon excitation. Opt Express 20(24):26219. https://doi.org/10.1364/OE.20.026219.
51. Christodoulou C et al (2020) Live-animal imaging of native haematopoietic stem and progenitor cells. Nature 578(7794):278–283. https://doi.org/10.1038/s41586-020-1971-z.
52. Becker W (2005) Advanced time-correlated single photon counting techniques. Springer, New York, NY
53. Jiménez-Banzo A, Ragàs X, Kapusta P, Nonell S (2008) Time-resolved methods in biophysics. 7. Photon counting vs. analog time-resolved singlet oxygen phosphorescence detection. Photochem Photobiol Sci 7(9):1003. https://doi.org/10.1039/b804333g
54. Rytelewski M et al (2019) Merger of dynamic two-photon and phosphorescence lifetime microscopy reveals dependence of lymphocyte motility on oxygen in solid and hematological tumors. J Immunother Cancer 7(1):78. https://doi.org/10.1186/s40425-019-0543-y.
55. Fricke M, Nielsen T (2005) Two-dimensional imaging without scanning by multifocal multiphoton microscopy. Appl Opt 44(15):2984. https://doi.org/10.1364/AO.44.002984.
56. Howard SS, Straub A, Horton NG, Kobat D, Xu C (2013) Frequency-multiplexed in vivo multiphoton phosphorescence lifetime microscopy. Nat Photonics 7(1):33–37. https://doi.org/10.1038/nphoton.2012.307
57. Denk W, Piston DW, Webb WW (1995) Two-photon molecular excitation in laser-scanning microscopy. In: Pawley JB (ed) Handbook of biological confocal microscopy. Springer, Boston, MA, pp 445–458
58. Larson DR (2003) Water-soluble quantum dots for multiphoton fluorescence imaging in vivo. Science 300(5624):1434–1436. https://doi.org/10.1126/science.1083780
59. Sakadžić S et al (2010) Two-photon high-resolution measurement of partial pressure of oxygen in cerebral vasculature and tissue. Nat Methods 7(9):755–759. https://doi.org/10.1038/nmeth.1490.
60. Fittinghoff DN, Wiseman PW, Squier JA (2000) Widefield multiphoton and temporally decorrelated multifocal multiphoton microscopy. Opt Express 7(8):273. https://doi.org/10.1364/OE.7.000273.

61. Spencer JA (2012) Characterization of bone marrow intravascular pO_2 by 2-photon phosphorescence quenching method. Doctoral Dissertation. Retrieved from ProQuest Dissertations and Theses (Accession Order No. AAT 3541737)
62. Lebedev AY, Cheprakov AV, Sakadžić S, Boas DA, Wilson DF, Vinogradov SA (2009) Dendritic phosphorescent probes for oxygen imaging in biological systems. ACS Appl Mater Interfaces 1(6):1292–1304. https://doi.org/10.1021/am9001698
63. Esipova TV, Karagodov A, Miller J, Wilson DF, Busch TM, Vinogradov SA (2011) Two new 'protected' oxyphors for biological oximetry: properties and application in tumor imaging. Anal Chem 83(22):8756–8765. https://doi.org/10.1021/ac2022234
64. Dunphy I, Vinogradov SA, Wilson DF (2002) Oxyphor R2 and G2: phosphors for measuring oxygen by oxygen-dependent quenching of phosphorescence. Anal Biochem 310:191
65. Wilson DF, Lee WMF, Makonnen S, Finikova O, Apreleva S, Vinogradov SA (2006) Oxygen pressures in the interstitial space and their relationship to those in the blood plasma in resting skeletal muscle. J Appl Physiol 101(6):1648–1656. https://doi.org/10.1152/japplphysiol.00394.2006
66. Lo L-W, Koch CJ, Wilson DF (1996) Calibration of oxygen-dependent quenching of the phosphorescence of Pd-meso-tetra (4-carboxyphenyl) porphine: a phosphor with general application for measuring oxygen concentration in biological systems. Anal Biochem 236 (1):153–160. https://doi.org/10.1006/abio.1996.0144
67. Roussakis E, Spencer JA, Lin CP, Vinogradov SA (2014) Two-photon antenna-core oxygen probe with enhanced performance. Anal Chem 86(12):5937–5945. https://doi.org/10.1021/ac501028m
68. Zlokovic BV (2011) Neurovascular pathways to neurodegeneration in Alzheimer's disease and other disorders. Nat Rev Neurosci 12(12):723–738. https://doi.org/10.1038/nrn3114
69. Montagne A, Zhao Z, Zlokovic BV (2017) Alzheimer's disease: a matter of blood–brain barrier dysfunction? J Exp Med 214(11):3151–3169. https://doi.org/10.1084/jem.20171406
70. Al-Bachari S, Vidyasagar R, Emsley HC, Parkes LM (2017) Structural and physiological neurovascular changes in idiopathic Parkinson's disease and its clinical phenotypes. J Cereb Blood Flow Metab 37(10):3409–3421. https://doi.org/10.1177/0271678X16688919
71. Lim RG et al (2017) Huntington's disease iPSC-derived brain microvascular endothelial cells reveal WNT-mediated angiogenic and blood-brain barrier deficits. Cell Rep 19(7):1365–1377. https://doi.org/10.1016/j.celrep.2017.04.021.
72. Devor A et al (2011) 'Overshoot' of O2 is required to maintain baseline tissue oxygenation at locations distal to blood vessels. J Neurosci 31(38):13676–13681. https://doi.org/10.1523/JNEUROSCI.1968-11.2011
73. Parpaleix A, Houssen YG, Charpak S (2013) Imaging local neuronal activity by monitoring PO2 transients in capillaries. Nat Med 19(2):241–246. https://doi.org/10.1038/nm.3059
74. Lecoq J et al (2011) Simultaneous two-photon imaging of oxygen and blood flow in deep cerebral vessels. Nat Med 17(7):893–898. https://doi.org/10.1038/nm.2394.
75. Sakadžić S et al (2014) Large arteriolar component of oxygen delivery implies a safe margin of oxygen supply to cerebral tissue. Nat Commun 5(1):5734. https://doi.org/10.1038/ncomms6734.
76. Kazmi SMS et al (2013) Three-dimensional mapping of oxygen tension in cortical arterioles before and after occlusion. Biomed Opt Express 4(7):1061. https://doi.org/10.1364/BOE.4.001061.
77. Kisler K et al (2017) Pericyte degeneration leads to neurovascular uncoupling and limits oxygen supply to brain. Nat Neurosci 20(3):406–416. https://doi.org/10.1038/nn.4489.
78. Lyons DG, Parpaleix A, Roche M, Charpak S (2016) Mapping oxygen concentration in the awake mouse brain. elife 5:e12024. https://doi.org/10.7554/eLife.12024
79. Roche M, Chaigneau E, Rungta RL, Boido D, Weber B, Charpak S (2019) In vivo imaging with a water immersion objective affects brain temperature, blood flow and oxygenation. elife 8: e47324. https://doi.org/10.7554/eLife.47324

80. Zhang Q et al (2019) Cerebral oxygenation during locomotion is modulated by respiration. Neuroscience. https://doi.org/10.1101/639419
81. Moeini M, Cloutier-Tremblay C, Lu X et al (2020) Cerebral tissue pO_2 response to treadmill exercise in awake mice. Sci Rep 10:13358. https://doi.org/10.1038/s41598-020-70413-3
82. Şencan İ, Esipova T, Kılıç K, Li B, Desjardins M, Yaseen MA, Wang H, Porter JE, Kura S, Fu B, Secomb TW, Boas DA, Vinogradov SA, Devor A, Sakadžić S (2020) Optical measurement of microvascular oxygenation and blood flow responses in awake mouse cortex during functional activation. J Cereb Blood Flow Metab. https://doi.org/10.1177/0271678X20928011
83. Rytelewski M, Harutyunyan K, Baran N, Mallampati S, Zal MA, Cavazos A, Butler JM, Konoplev S, El Khatib M, Plunkett S, Marszalek JR, Andreeff M, Zal T, Konopleva M (2020) Inhibition of oxidative phosphorylation reverses bone marrow hypoxia visualized in imageable syngeneic B-ALL mouse model. Front Oncol 10:991. https://doi.org/10.3389/fonc.2020.00991
84. Şencan I et al (2018) Two-photon phosphorescence lifetime microscopy of retinal capillary plexus oxygenation in mice. J Biomed Opt 23(12):1. https://doi.org/10.1117/1.JBO.23.12.126501
85. Kritchenkov IS, Elistratova AA, Sokolov VV, Chelushkin PS, Shirmanova MV, Lukina MM, Dudenkova VV, Shcheslavskiy VI, Kalinina S, Reeß K, Rück A, Tunik SP (2020) A biocompatible phosphorescent Ir(iii) oxygen sensor functionalized with oligo(ethylene glycol) groups: synthesis, photophysics and application in PLIM experiments. New J Chem 44(25):10459–10471. https://doi.org/10.1039/D0NJ01405B
86. Schilling K et al (2019) Electrospun fiber mesh for high-resolution measurements of oxygen tension in cranial bone defect repair. ACS Appl Mater Interfaces 11(37):33548–33558. https://doi.org/10.1021/acsami.9b08341.